



HAL
open science

Design, optical characterization, and operation of large transmission gratings for the laser integration line and laser megajoule facilities

Jerome Neauport, Eric Journot, Gaël Gaborit, Philippe Bouchut

► **To cite this version:**

Jerome Neauport, Eric Journot, Gaël Gaborit, Philippe Bouchut. Design, optical characterization, and operation of large transmission gratings for the laser integration line and laser megajoule facilities. Applied optics, 2005, pp.3143-3152. 10.1364/AO.44.003143 . cea-01053356

HAL Id: cea-01053356

<https://cea.hal.science/cea-01053356>

Submitted on 30 Jul 2014

HAL is a multi-disciplinary open access archive for the deposit and dissemination of scientific research documents, whether they are published or not. The documents may come from teaching and research institutions in France or abroad, or from public or private research centers.

L'archive ouverte pluridisciplinaire **HAL**, est destinée au dépôt et à la diffusion de documents scientifiques de niveau recherche, publiés ou non, émanant des établissements d'enseignement et de recherche français ou étrangers, des laboratoires publics ou privés.

Design, optical characterization, and operation of large transmission gratings for the laser integration line and laser megajoule facilities

Jérôme Néauport, Eric Journot, Gaël Gaborit, and Philippe Bouchut

Within the framework of the laser integration line (LIL) and the laser megajoule, we describe the design, optical characterization, mounting, alignment, and operation on the LIL of large $420\text{ mm} \times 470\text{ mm}$ transmission gratings. Two types of grating were manufactured. The first, operating at a wavelength of $1.053\text{ }\mu\text{m}$, was used for deviation purposes. The second, operating at a wavelength of $0.351\text{ }\mu\text{m}$, was used for both deviation and focusing purposes. We demonstrate that these large transmission gratings are suitable for nanosecond-regime operation on high-power laser facilities. © 2005 Optical Society of America

OCIS codes: 140.0140, 050.1950, 080.3630, 220.4840.

1. Introduction

In fusion-class laser systems, such as the laser megajoule¹ (LMJ) or National Ignition Facility (NIF),² the energy transported by large laser beams needs to be focused on a small target of a size of approximately 1 mm at the wavelength of $0.351\text{ }\mu\text{m}$. The LMJ will thus be equipped with 240 beams having a section of $400\text{ mm} \times 400\text{ mm}$. Each laser line will be constituted of 40 large optical components. The amplification as well as the transport of the large laser beams are made at a wavelength of $1.053\text{ }\mu\text{m}$ (called 1ω). Frequency conversion at $0.351\text{ }\mu\text{m}$ (called 3ω) and focusing are subsequently performed. The design and building of optical elements ensuring the focusing of such powerful laser beams have to take into account various constraints. As Latkowski *et al.*³ recently pointed out, limiting the exposure of the final optics assembly to laser-induced high-energy neutrons and gamma rays is a key issue for limiting maintenance cost of this expensive end part of the laser line. There-

fore, since 1994 we have worked out focusing solutions that satisfy this constraint. Since laser-target interaction is performed at 3ω , the residual 1ω and 2ω remaining after frequency conversion must be separated from the main 3ω laser beam. For most of the laser-target vacuum chamber space to be used for diagnostics, it was necessary to perform this wavelength separation before the beam enters the chamber. Let us now focus on the optical component involved in the laser beam focusing. To minimize the final focal spot size, limit the laser line cost, and facilitate maintenance operations, we restricted to one or two the number of optics involved in focusing. Note that for high-power lasers, high damage threshold optics are needed. The typical fluence specification for optics operating at $0.351\text{ }\mu\text{m}$ ranges from 10 to 16 J/cm^2 , depending on the position of these optics within the laser line. Taking into account alignment uncertainty, optics aberrations, and stability considerations of the laser lines, we show that the optics guaranteeing the focusing function have to be almost diffraction limited at their operating wavelengths. On the basis of these considerations, reflective, refractive, or diffractive solutions have been sought.

Our refractive solutions used mirrors to focus the light at a wavelength of $0.351\text{ }\mu\text{m}$. Though this principle have been already applied on other laser drivers,⁴ we found out that using a combination of a plane mirror and a parabolic focusing mirror for our system led us to cumbersome solutions. Moreover, despite the latest significant progress made, high-reflection

J. Néauport (jerome.neauport@cea.fr), E. Journot, and G. Gaborit are with the Commissariat à l'Energie Atomique, Centre d'Etudes Scientifiques et Techniques d'Aquitaine, BP2, Le Barp Cedex, France, 33114. P. Bouchut is with the Commissariat à l'Energie Atomique Laboratoire d'Electronique de Technologie de l'Information, 17 rue des Martyrs, 38054 Grenoble Cedex 9, France.

Received 12 July 2004; revised manuscript received 27 October 2004; accepted 5 November 2004.

0003-6935/05/163143-10\$15.00/0

© 2005 Optical Society of America

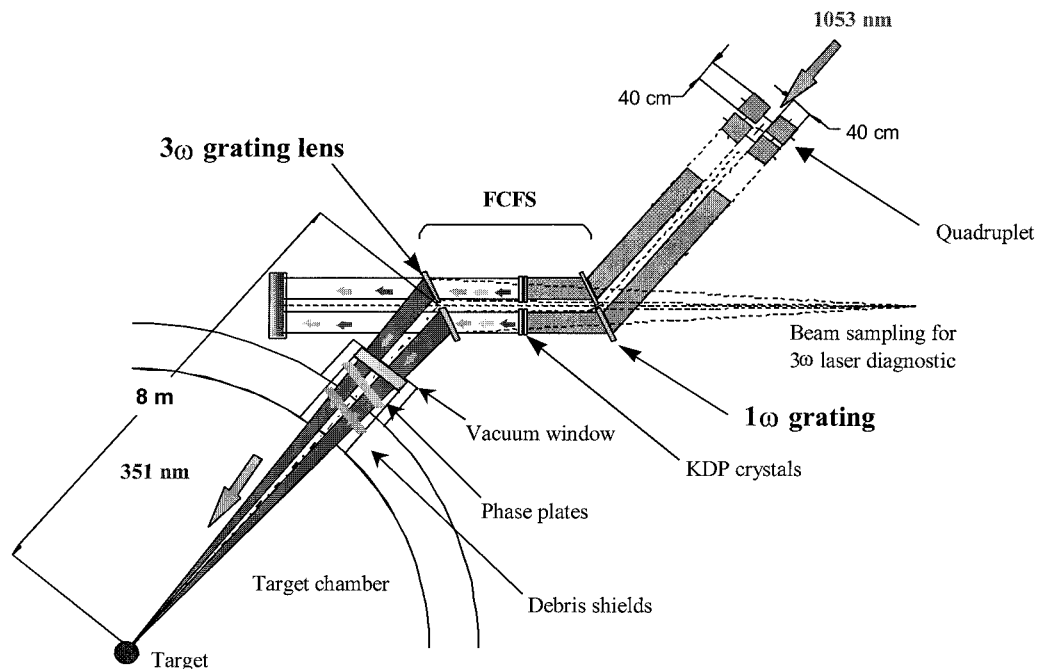


Fig. 1. Final optics assembly design of the LIL and LMJ.

coatings based on fluoride materials could not sustain high fluence at $0.351\ \mu\text{m}$ and had rather complex coating designs.⁵ Hence, they were discarded.

Refractive designs used an aspheric prismatic lens to focus the 3ω light at the center of the vacuum chamber. Taking into account the neutrons isolation and the wavelength separation constraints, the refractive designs led us to complex solutions and were therefore dismissed. Designs based on diffractive elements were compatible with our constraints and led us to the final optics assembly baseline depicted in Fig. 1. Focusing and wavelength separation is made by a focusing grating called the 3ω grating. This grating is equivalent to a very chromatic off-axis lens and is introduced after the frequency conversion completed by KDP crystals. Since it is used in a diffracted order, the 3ω grating introduces an optical path difference between top and bottom rays that must be compensated, if laser-pulse-width broadening is to be avoided. This is done by a second grating, called the 1ω grating, working at a wavelength of $1.053\ \mu\text{m}$ and located just before the KDP crystals. Resorting to these two diffractive optics led us to this zigzag setup and enabled isolation from neutrons and gamma rays to be performed. Moreover, since the laser is used in broad spectral bandwidth for beam-smoothing purposes,⁶ dispersion of the 1ω grating enhances the KDP conversion yield because the phase-matching angle of each wavelength on the KDP crystals is adapted.⁷ Another advantage of the diffractive method is due to the holographic nature of the 3ω grating. By construction, this grating features a focused reflected order that can be used for laser line focal spot diagnostic.

We herein present the developments we have achieved to have our gratings operational in our final

optics assembly. The design of these two diffractive components is depicted in Section 2. Final specifications and some manufacturing considerations are detailed in Section 3. Optical metrology of the components and results are presented in Section 4. Finally, we present data obtained on the laser integration line (LIL). This 1/60 scale prototype of the LMJ, equipped with 8 laser beams of full aperture, used the manufactured gratings.

2. Design of the 1ω and 3ω Gratings

Designs of 1ω and 3ω gratings are very similar. The following discussion is mainly based on the 1ω grating design. Transposition to the 3ω grating is briefly discussed at the end of this section. Since the purpose of large-laser fusion facilities is to bring the maximum amount of energy onto the target, the losses incurred by the gratings must be as low as possible. We thus want a diffraction efficiency of more than 90%. Moreover, high damage threshold optics in UV are needed. Therefore, pure fused-silica optics are necessary. Accordingly, the only affordable gratings are engraved on fused silica.

The main task was then to draw a highly efficient grating operating in TM polarization (the plane of polarization of the \mathbf{E} vector is in the plane of incidence). This polarization was retained for conversion frequency considerations.⁷

The basic geometric law of diffraction grating relates the incident (i_1) and diffraction (i_p) angles with the wavelength (λ) and period of the grating (Λ) [see Fig. 2 and Eq. (1)]. We use the notation $-pR$ for reflected orders and $-pT$ for transmitted orders.

$$\sin i_1 + \sin i_p = -p \lambda / \Lambda \quad (1)$$

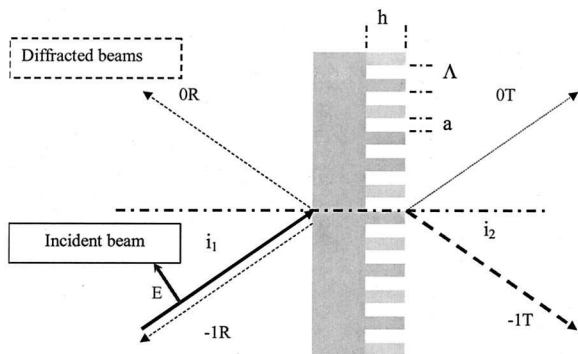


Fig. 2. Operational configuration of the transmission grating.

To achieve high diffraction efficiency in a specific order, it is necessary to minimize the number p of orders in which the energy can be diffracted. However, diffraction by phase discontinuity of the refractive profile structure implies that all available orders contain energy, even though a refractive profile for one specific order is optimized. If Λ is greater than 20λ , diffraction is well described by geometric analysis of phase in the various diffracted waves, and for smaller Λ , we need to solve Maxwell's equations in the periodic structure to assess the diffraction efficiency of each diffracted order. It is very difficult to experimentally achieve more than 80%–85% of diffraction efficiency in one specific order with this kind of grating. This experimental fact is consistent with the well-known energy contained in the first ring of the diffraction figure of a circular pupil. Hence, to reach our goal of 90% diffraction efficiency in 1 order, we must design a grating with Λ close to λ since Eq. (1) shows that p values can yet only be $-1, 0, 1$.

As previously demonstrated,^{8,9} symmetrical diffracting profiles with a symmetrical operational configuration are likely to maximize the energy diffraction in 1 order. By choosing the angle of incidence to eliminate the $p = 1$ solution, we obtain 2 orders accessible to the diffracted energy: $p = 0$ or $p = -1$. Given that our gratings operate in transmission, the reflected orders will have an efficiency less or equal to Fresnel's reflection coefficient. The period of the grating being close to the wavelength, the apparent index of the grating profile is averaged between glass and air indexes. In fact, the grating profile behaves like an antireflection coating deposited on the bulk glass substrate and induces the efficiency of reflected orders to be very small (less than 1%). Our last degree of freedom to optimize the $p = -1$ T order in terms of diffraction efficiency is the geometry of the grating profile. This geometry is defined by the type of profile (triangle, square. . .), the depth of the grooves (h) and the duty cycle (DC) [Eq. 2].

$$DC = (\Lambda - a)/\Lambda. \quad (2)$$

We then must solve Maxwell's equations for the retained grating, optimizing h to achieve the best dif-

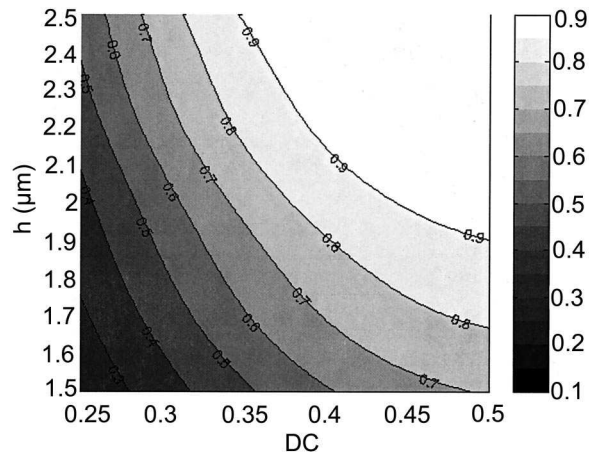


Fig. 3. Diffraction efficiency in the $-1T$ order, 30° incidence, TM, and wavelength of $1.053 \mu\text{m}$.

fraction efficiency of the $-1T$ order. To perform that, the GSOLVER code was used.¹⁰ This code is dedicated to diffraction calculation for every kind of grating and was run on a desktop PC. By our setting all the parameters of the grating (wavelength, grating period and profile, DC, depth, material index and absorption, and polarization state of the incident wave) except for a variable one, the code calculates the diffraction efficiency of all the orders for a given value of the variable. Using this procedure, we find a theoretical value of h that achieves 100% of the transmitted diffracted energy in the $-1T$ order. For most cases, the depth of the profile is approximately 2–3 times the period of the grating.

We have to keep in mind that we must manufacture a lamellar grating in fused silica with a spatial period of approximately $0.35 \mu\text{m}$ for the 3ω grating. The holographic recording process, detailed in Section 3, is the only one producing large optical components with such fine structures. All the manufacturing steps of this process need a lot of care, but the etching one is the most difficult to achieve. Therefore, to loosen the design constraints, one has to minimize the grating profile depth. Furthermore, the holographic recording and etching make a square profile easier to achieve.

Accordingly, we determined the optimum depth of the structure for a DC of 0.5 and then checked the sensitivity of diffraction efficiency with respect to small variation of depth, DC, incident angle, wavelength, and index. Using GSOLVER, we have found that whatever the profile, the minimal depth is achieved for $DC = 0.5$. The minimum depth is obtained for a square profile but with a tiny loss of efficiency.

Although Kogelnik⁸ has shown that the best configuration to optimize the $-1T$ order is $i_1 = i_{-1} = 30^\circ$, $\lambda = \Lambda = 1.053 \mu\text{m}$, we have found that this configuration leads to quite deep gratings (Fig. 3). We were seeking the least-sensitive operating configuration with respect to fabrication parameters (h , DC), with more than 90% efficiency and the smallest possible depth. The only parameter that can change is

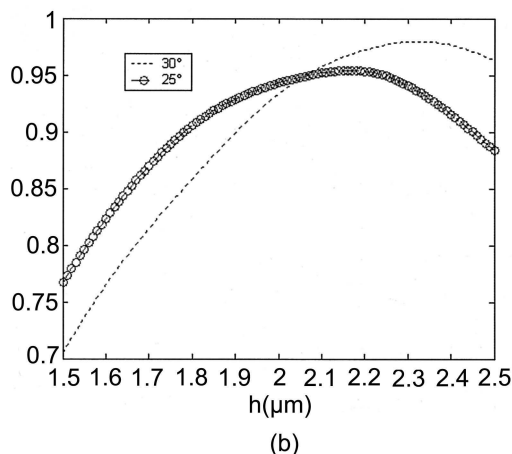
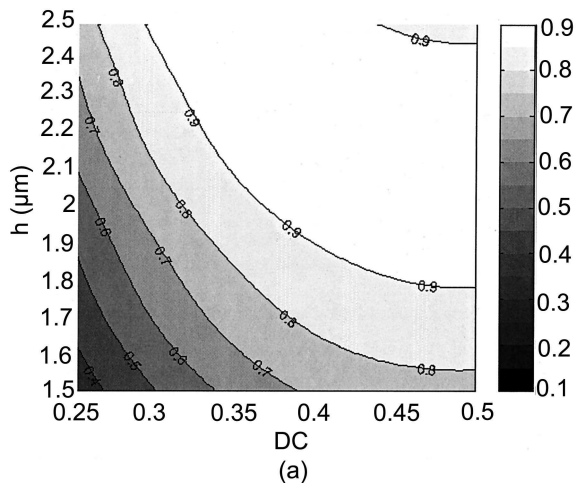


Fig. 4. (a) Diffraction efficiency in the $-1T$ order, 25° incidence, TM, and wavelength of $1.053 \mu\text{m}$ (b) 30° and 25° gratings diffraction efficiency $-1T$ order TM for $DC = 0.5$.

the incident angle, and a more robust operational configuration is obtained for an incident angle of 25° . In Fig. 4 a typical diffraction efficiency abacus for variables (h , DC) for such a 1ω grating operating at 25° in TM is shown and compared to the 30° solution for $DC = 0.5$.

The final theoretical 1ω grating retained configuration is

$$\begin{aligned} \lambda &= 1.053 \mu\text{m}, \\ i &= 25^\circ, \\ \Lambda &= 2.4564 \mu\text{m} \text{ (groove density of } 803.019 \text{ g/mm)}, \\ h &= 2.1 \mu\text{m}, \\ DC &= 0.4 \text{ to } 0.5, \\ \text{Diffraction efficiency} &> 90\%. \end{aligned}$$

The design of the 3ω grating is very similar:

$$\begin{aligned} i &= 25^\circ \text{ (same incident angle to compensate the optical path difference),} \\ \lambda_{3\omega} &= \lambda_{1\omega}/3, \\ \Lambda_{3\omega} &= \Lambda_{1\omega}/3 \text{ (groove density of } 2409.058 \text{ g/mm)}, \\ h_{3\omega} &= h_{1\omega}/3, \\ DC &= 0.4 \text{ to } 0.5, \\ \text{Diffraction efficiency} &> 90\%. \end{aligned}$$

The major characteristic of the 3ω grating is that it is a focusing grating. To achieve focusing one needs to modify the holographic recording configuration as described in next section in order to obtain slightly curved and no equispaced grooves.

3. Specifications for the 1ω and 3ω Gratings

On the basis of the work presented in Section 2, the specifications detailed in Table 1 were selected for the 1ω and 3ω LIL/LMJ gratings. Diffracted $-1T$ wave-front quality is specified in terms of encircled energy for the 3ω focusing grating. For the 1ω grating, we have specified the curvature of the wave front in the

Table 1. 1ω and 3ω Gratings Specifications

Specification	Gratings	
	1ω	3ω
Wavelength (μm)	1.053	0.351
Polarization	TM	TM
Substrate	Fused silica	Fused silica
Dimensions	420 mm \times 470 mm	420 mm \times 470 mm
Clear aperture	400 mm \times 450 mm	400 mm \times 450 mm
Incidence	25°	25°
Deviation for the geometric center of the quadruplet	50°	50°
Focal distance	-	8 m
Efficiency in the $-1T$ order	$>90\%$	$>90\%$
Efficiency in the $-1R$ order	-	$>1\%$
Damage threshold for 3-ns pulses at $1.053 \mu\text{m}$	$>25 \text{ J/cm}^2$	-
Damage threshold for 3-ns pulses at $0.351 \mu\text{m}$	-	$>12 \text{ J/cm}^2$
Focal spot encircled energy (diameter)	-	90% $< 50 \mu\text{m}$ 95% $< 90 \mu\text{m}$
Transmitted wave-front quality on clear aperture	Curvature $< 1 \mu\text{m}$ Max. Slope $< 5 \mu\text{rad}$	-

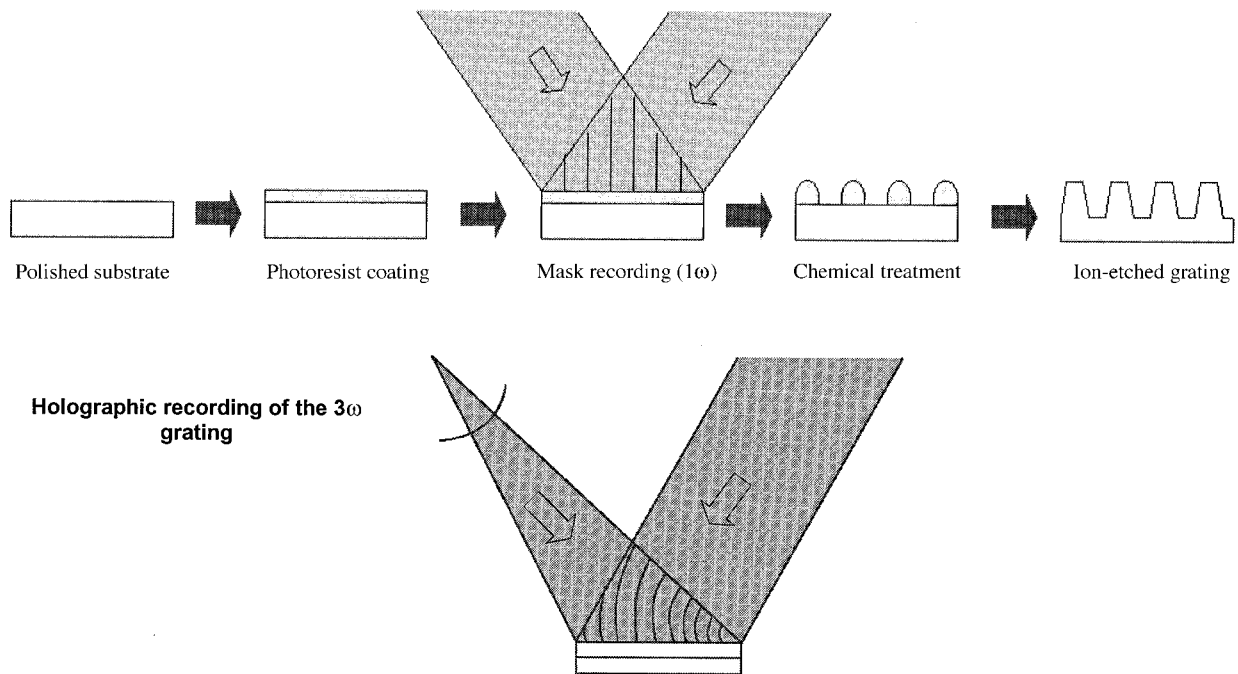


Fig. 5. Grating manufacturing process.

–1T order. We have also specified the maximal slope of this diffracted wave front in microradians after suppressing the wave-front curvature.

Grating manufacturing was done by Jobin Yvon using a conventional holographic process (Fig. 5). A polished substrate is covered with a photosensitive resin. The latter is exposed onto a holographic bench. The pattern generated by the interference of two plane wave fronts is used for recording the 1ω grating. A plane and a spherical wave front are used to introduce the focusing property of the 3ω grating. The exposed photosensitive layer is then developed to display grooves in relief on the substrate. This structure is then transferred into the fused-silica substrate by an ion-etching process.

4. Gratings Characterization

A. Wave-Front Quality

To check the power and maximum slope of a transmitted wave front in the first order of the 1ω grating, we use a ZYGO interferometer set with an 800-mm expander. This interferometer is equipped with a modified ZYGO MARK IV mainframe operating at $1.064\ \mu\text{m}$. Two reference flats are used (800-mm diameter, flatness close to $60\ \text{nm}$ on a $400 \times 400\ \text{mm}^2$ aperture). The phase map is achieved as a result of the interferometer using a software called FLIP,¹¹ which is based on a spatial linear carrier analysis.¹² With this method 1 interferogram of approximately 50 fringes (tilt between the reference and the transmitted wave front) is needed to calculate the phase map of the wave front. Therefore, it has the advantage of being slightly sensitive to vibration, compared with the phase-shifting method. It

enables us to measure large components without moving a large reference flat with a piezoelectric. We obtained the measured wave front by averaging 50 interferograms with 2 opposite tilts. However, the measurement tilt limits the spatial resolution to a period greater than $10\ \text{mm}$. The analysis of the phase map is made by a software called Anaphase.¹³ This software is used by all LIL/LMJ optics manufacturers and computes all parameters of the specified wave front [power, peak to valley (p.v.), rms, slope, etc.].

A typical 1ω grating –1T order transmitted wave front is shown in Fig. 6. The wave-front curvature is

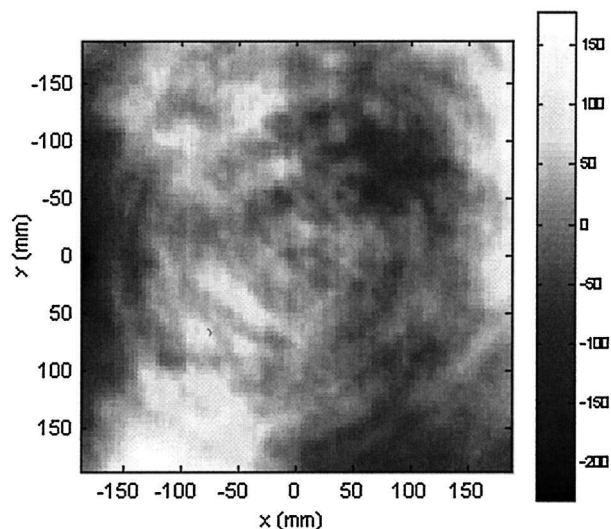


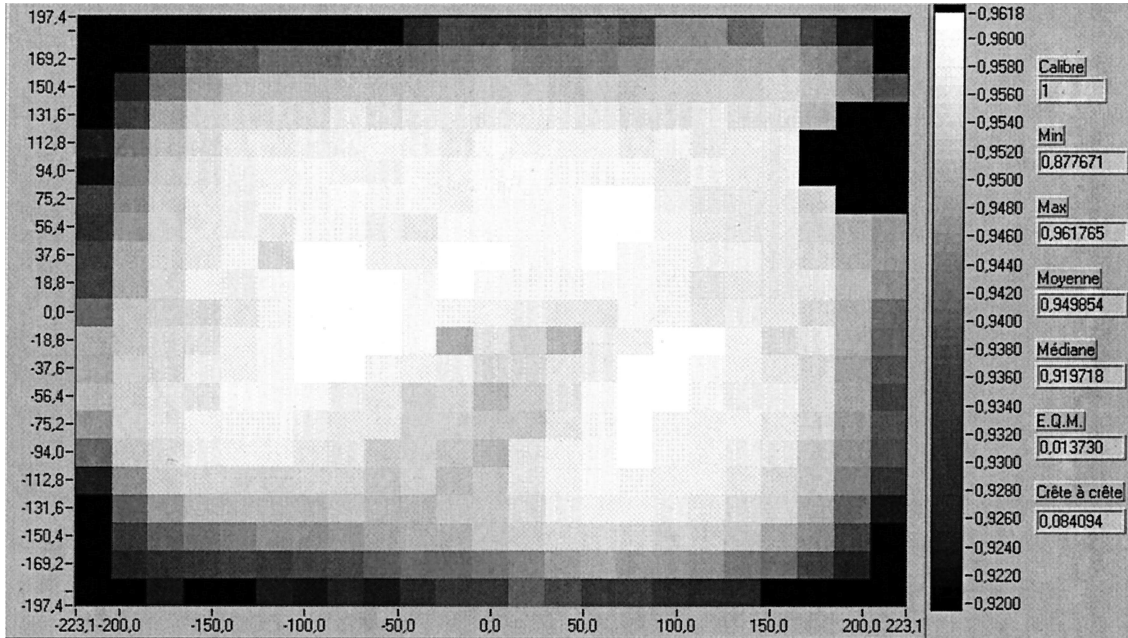
Fig. 6. Transmitted wave front of a 1ω grating (00-0007) in nanometers, –1T order, 1.064-m wavelength, TM polarization. Power, $110\ \text{nm}$; p.v. without power, $410\ \text{nm}$; maximum slope, $9\ \mu\text{rad}$.

Table 2. Focal Spot Analysis of 3- ω Grating

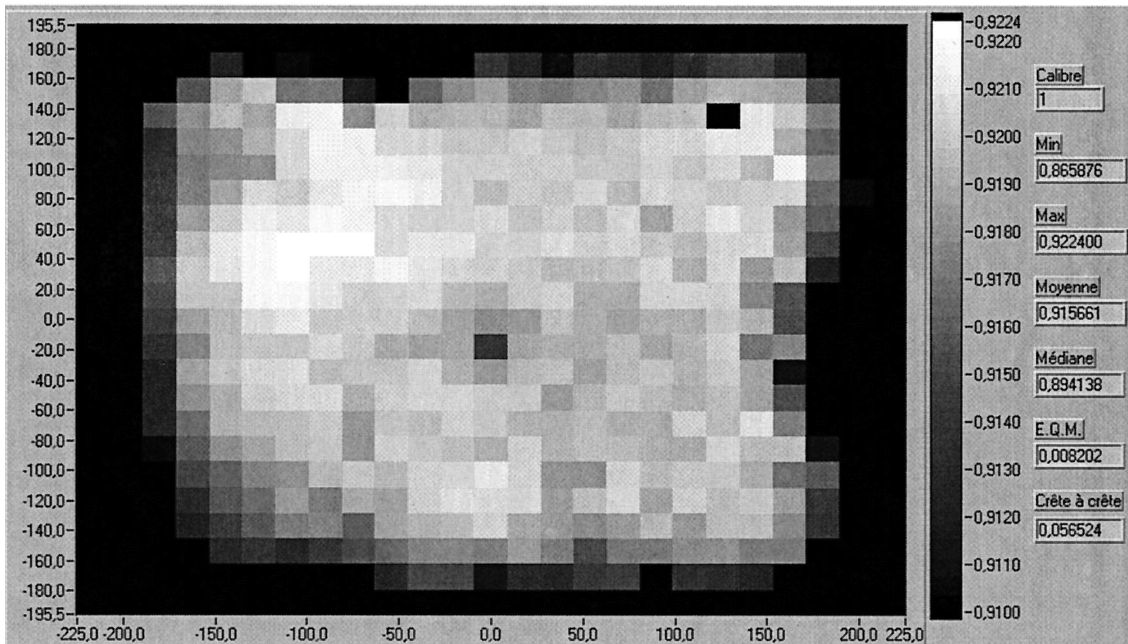
Focal spot encircled energy diameter	00-0006 (μm)	Specification (μm)
>90%	57	50
>95%	92	90

far below Commissariat à l'Énergie Atomique (CEA) specification. We have noticed that a residual amount of aberrations has been introduced during the grating recording. The maximal slope is beyond CEA's specification. However, since the defect is located at the edge of the clear aperture, the component can be used without problems.

The 3 ω grating -1T order focal spot is also a good indication of the wave-front quality. This focal spot



(a)



(b)

Fig. 7. (a) Efficiency of a 1 ω grating (99-0135), -1T order, 1.053- μm wavelength, and TM polarization. (b) Efficiency of a 3 ω grating (CH03-03), -1T order, 0.351- μm wavelength, and TM polarization.

was measured in operating conditions by Jobin Yvon. Some findings obtained on a 3ω grating are given in Table 2. The measured focal spot is very close to CEA's specification. Other far-field images of the 3ω grating have been also detailed before.⁶

B. Diffraction Efficiency

We have developed a specific photometer together with Société Européenne des Systèmes Optiques Company¹⁴ in order to check the photometric characteristics of our gratings. This device is a single-point scanning system. The beam ($\varnothing \sim 5$ mm at $1/e$ in intensity) is stationary while the undergoing component moves parallel to its surface. The photometer uses two detectors:

- a reference detector, monitoring laser power variations during scanning (approximately 30 min),
- a signal detector, measuring transmission or reflection powers.

The signal detector follows the beam during the scanning motion. This point is significant for the 3ω grating since the local deviations vary all along the scanned surface.

A calibration is made before each measurement by use of the transmission through air for a coefficient close to 1 or a reflection on a fused-silica plate for a coefficient close to 0.01. The photometer performs measurements with two linear polarizations (TM or TE) at three wavelengths (1.053, 0.5265, and 0.351 μm) delivered by a unique Q-switched laser. The estimated absolute accuracy of the photometer is 0.002 ($k = 3$) for a coefficient close to 1 and 0.0002 ($k = 3$) for a coefficient close to 0.01.

With this setup, it was possible to measure the diffraction efficiency of various gratings by scanning the clear aperture, with a sampling step of 20 mm \times 20 mm in their -1T order at their operating wavelength in TM polarization. Figure 7(a) shows the efficiency map obtained for a 1ω grating. The substrate on which the grating was etched had a solgel coating deposited on the other side. Figure 7(b) shows the efficiency map obtained on a 3ω grating sample. The back side of the substrate was not solgel coated and therefore, the Fresnel losses have not been taken into account (approximately 2.5%). In both cases, excellent diffraction efficiencies were measured with mean values of approximately 95.0% for the 1ω grating and 93.9% for the 3ω grating (Fresnel losses of the back side deducted).

C. Laser-Induced Damage Threshold

We measured laser-induced damage threshold at the wavelength of 1.064 μm for the 1ω grating and 0.355 μm for the 3ω grating by using an automated damage test facility that has been described previously.¹⁵ Multiple pulses of increasing energy were sent on a site until scattering was detected by a diagnostic with a He-Ne laser source. A ramp-on-site (R/1) procedure was employed. During this procedure, more than 200 sites were tested on a 100-mm

Table 3. Laser-Induced Damage Threshold of a 1ω Grating Compared with the Threshold of a Polished Sample without Grating Engraved^a

Sample Type	Minimum (J/ cm ²)	Mean (J/ cm ²)	Maximum (J/ cm ²)
Polished sample	34	113	213
1ω grating sample	25	90	156

^aR/1 testing mode, 1.064 μm , 3 ns.

grating sample, giving access to the statistical weight of the peak fluence at which the damage occurred. Minimal, mean, and maximal values of this statistical repartition were then computed. Testing at 1.064 μm was made with a Coherent Infinity laser with a pulse duration of 3 ns, the laser beam surface on the sample being equivalent to a Gaussian beam of 0.2 mm². Testing at 0.355 μm required use of a Spectra Physics GCR-350 laser source with a pulse duration of 6.8 ns, the laser beam surface on the sample being 0.02 mm². Data gathered during measurement at 0.355 μm were rescaled for 3-ns pulse duration by use of the $\tau^{0.5}$ scaling factor.¹⁶ Samples were measured at their working incidence in TM polarization, with grating surface being placed on the exit surface of the laser beam. The R/1 damage testing procedure was chosen because it was convenient for small samples. Moreover, it is a reliable indicator for the improvement of the damage threshold all along the grating manufacturing process development. Note that it is not a direct indicator of the optics lifetime for the 3ω grating operating at 0.351 μm since lifetime is governed at this wavelength both by damage initiation and by damage growth.¹⁷

Tables 3 and 4 present our findings. To evaluate the effect of grating manufacturing, we compared the results with those of a polished sample with no grating engraved. Minimal threshold of the 1ω grating (25 J/cm²) is compatible with our specification. However, grating manufacturing induces a degradation of the performances of the original finished substrate. Up to now, we have not been able to account for this phenomenon or to relate it to a specific manufacturing process step of the grating. As we have not noticed any evolution of the 1ω grating operating on LIL (see Subsection 4.B), this problem has not been further investigated. As described before by Nguyen *et al.*,¹⁸ the 3ω grating performances are limited by the polished substrate. Besides, we have noticed an improvement of both mean and maximal values of the damage threshold on the 3ω grating. This improvement has been at-

Table 4. Laser-Induced Damage Threshold of a 3ω Grating Compared with the Threshold of a Polished Sample without Grating Engraved^a

Sample Type	Minimum (J/ cm ²)	Mean (J/ cm ²)	Maximum (J/ cm ²)
Polished sample	10,5	16	26
3ω grating sample	10,5	29	50

^aR/1 testing mode, 0.355 μm , data rescaled for 3-ns pulses.

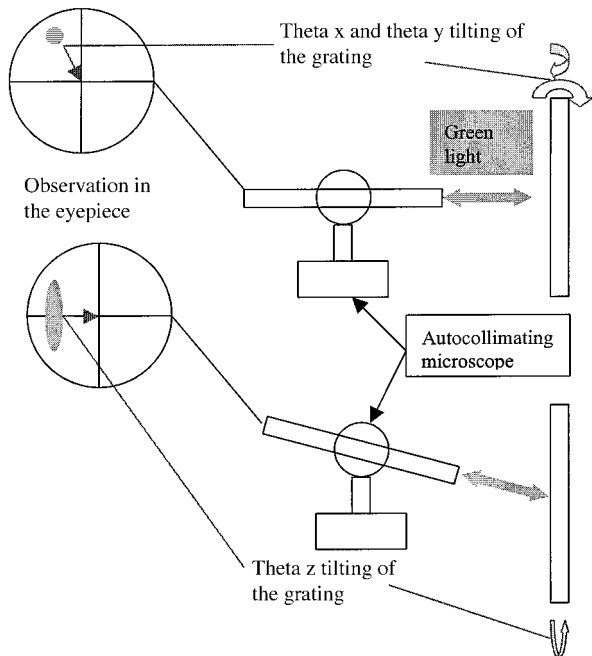


Fig. 8. Grating alignment principle.

tributed to the etching process of the grating. The lifetime at 351 nm of fused-silica optics will probably be essentially affected by surface flaws and contaminants left by polishing processes. Growth of laser-induced damage initiated at these defects is

the key factor of the operational durability of any fused-silica optics, including gratings.

5. Operation of the 1ω and 3ω gratings on the Laser Integration Line

A. Integration and Alignment Principles of the Grating

As explained in Section 1, the final optics assembly must focus four UV beams on a single point. To achieve this and to avoid any problem related to ghost beams, one needs to correctly align the 1ω and 3ω gratings in x - y and z and theta x and theta y directions.

The angular tuning of the 1ω gratings has been performed with a high-precision theodolite. We tuned theta x and theta y alignment by observing the classic 0R reflection order of the grating and the theta z alignment thanks to the $-1R$ order (Fig. 8). At the end of this process, the four 1ω gratings are parallel to one another within a tolerance of 10 s of arc in each angular direction. The group of 1ω gratings has then been integrated in the final optics assembly.

The alignment of the 3ω gratings is more complicated and has been done in two steps. The first step was very similar to the 1ω grating alignment, whereas the second step was performed through a wave-front sensor. Alignment has been carried out with the final optics assembly mounted on its alignment bench. An optical fiber, lit by a 3ω laser, illuminates the final optics assembly and acts as a 3ω

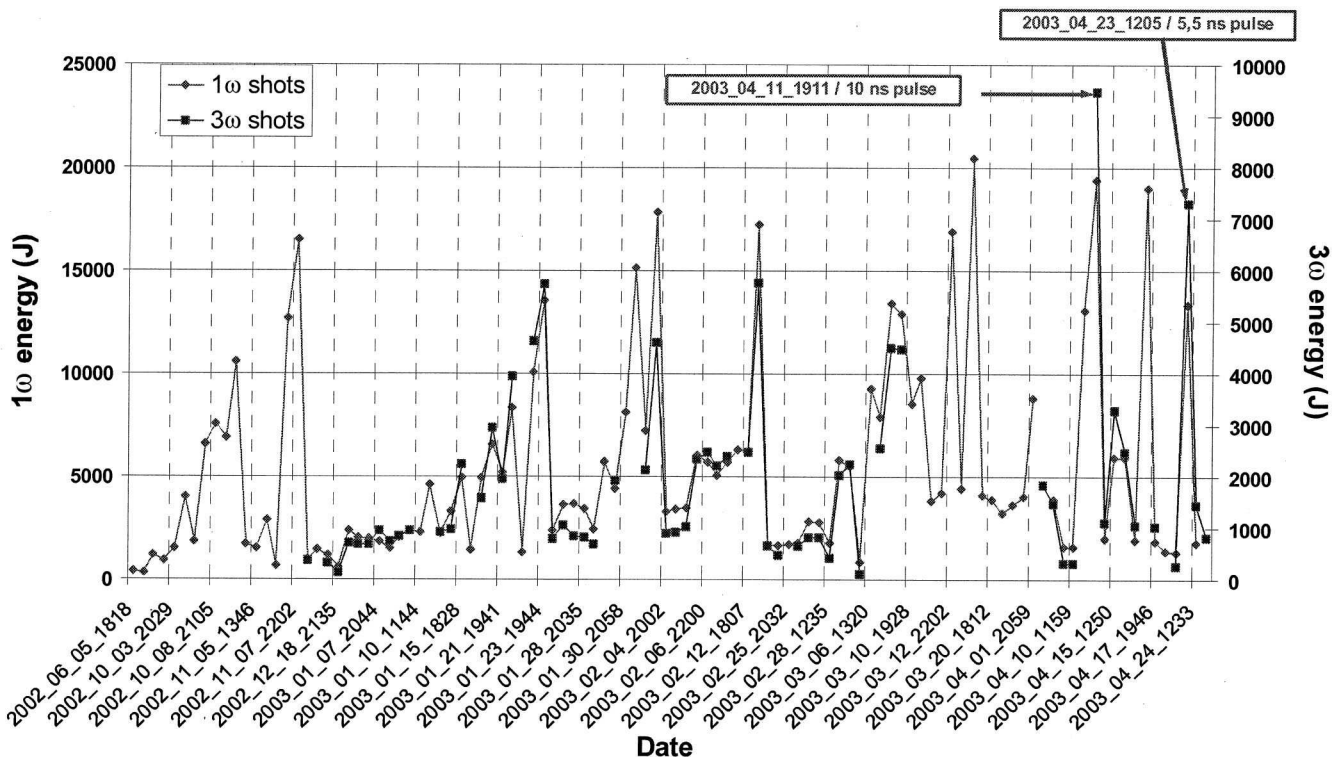


Fig. 9. Shots energy and chronology. LIL campaign (one beam line) from 2 June to 3 April. Energy at 1.053 and 0.351 μm for each shot.

Table 5. Evolution of the Diffraction Efficiency of the 3- ω Grating before and after LIL Campaign on a Centered $300 \times 280 \text{ mm}^2$ portion of the Clear Aperture^a

Status	-1T Order Efficiency at $0.351 \mu\text{m}$
Before campaign	$94.1\% \pm 0.4\%$
After campaign	$94.5\% \pm 0.4\%$

^aGrating's substrate backside AR coated.

point source. This diverging beam is collimated by the 3ω gratings, diffracted in the $-3T$ order by the 1ω gratings, then reflected back by a mirror (which is the alignment reference of the final optics assembly), diffracted again by the 1ω gratings, and finally focused by the 3ω gratings. The position of each focal spot has been tuned by translation of the 3ω gratings in x - y - z alignment. Tilting the 3ω gratings tuned the focal spot quality. The wave-front analysis has been done in the vicinity of $-1T$ foci.

As noted before, $-1R$ foci also exist, and the superimposition of the four $-1R$ focal spots has been checked at each step of the alignment process.

When the alignment of the final optics assembly has been completed

- i. the focused $-1T$ beams are superimposed to the 3ω source point with a quality close to the diffraction limit,
- ii. the focused $-1R$ beams are superimposed.

B. Operation of the Gratings on the Laser Integration Line Ramp-Up Campaign

During the characterization of the LIL laser performances, we have explored an energy/power diagram with specific points: 2 TW/700 ps, 7.3 kJ/5 ns, and 9.5 kJ/9 ns (Fig. 9). Both 1ω and 3ω gratings operating on the LIL have been observed and measured before and after the shot campaign. We have not noticed any significant evolution of the 1ω grating despite shots at more than 15 kJ sustained by this grating during the campaign. Regarding the 3ω grating, some damage appeared on the grating surface with a good correlation with the position of the laser beam hot spots. This damage was typical of that generated on fused-silica polished surfaces at the wavelength of $0.351 \mu\text{m}$. Our conclusions, supported by experiments described in Subsection 4.C, are that damage is induced by weak points of the finished substrate before grating manufacturing. Moreover, a measurement of the diffraction efficiency of the 3ω grating at the wavelength of $0.351 \mu\text{m}$ in its $-1T$ order revealed no significant evolution of the efficiency as shown on Table 5.

6. Conclusion

Although 100% diffraction efficiency gratings have been put forward before, we have suggested a new design of gratings, making the production of large-size optics possible with a diffraction efficiency of more than 90%. These optics are made by use of a conventional holographic process and present high

damage thresholds at both 1ω and 3ω . These components permit the laser beam to be focused with a quality similar to that of an aspheric lens. We have also described an alignment procedure that makes it possible to focus four 3ω laser beams onto the same focal spot. The very good performances achieved in our laboratory have been confirmed during the LIL operation. More than 40 1ω and 3ω large gratings have been successfully produced and tested, thus demonstrating the relevance of diffractive optics for large-power laser facilities.

We acknowledge J. Flamand, F. Bonnemason, G. de Villèle, Y. Josserand, S. Kaladgew, P. Gacoin, and the entire Jobin Yvon LIL/LMJ manufacturing team for their enduring enthusiasm, efforts, and competence during the development and production of LIL gratings. We thank also J. Paye, who was at the origin of the grating focusing idea in 1994.

References

- M. L. André, "Status of the LMJ project," in *Solid State Lasers for Application to Inertial Confinement Fusion: Second Annual International Conference*, M. L. André, ed., Proc. SPIE **3047**, 38–42 (1996).
- W. H. Lowdermilk, "Status of the National Ignition Facility project," in *Solid State Lasers for Application to Inertial Confinement Fusion: Second Annual International Conference*, M. L. André, ed., Proc. SPIE **3047**, 16–37 (1996).
- J. F. Latkowski, Alison Kubota, M. J. Caturla, S. N. Dixit, J. A. Speth, and S. A. Payne, "Fused silica final optics for inertial fusion energy: radiation studies and system-level analysis," *Fusion Technol.* **43**, 540–558 (2003).
- R. L. Bieri and M. W. Guinan, "Grazing incidence metal mirrors as the final elements in a laser driver for inertial confinement fusion," *Fusion Technol.* **19**, 673–678 (1991).
- J. Dijon, E. Quesnel, B. Rolland, P. Garrec, C. Pelle, and J. Hue, "High-damage threshold fluoride UV mirrors made by ion-beam sputtering," in *Laser-Induced Damage in Optical Materials: 1997*, G. J. Exarhos, A. H. Guenther, M. R. Kozlowski, and M. J. Soileau, eds., Proc. SPIE **3244**, 406–416 (1998).
- J. Néauport, X. Ribeyre, J. Daurios, D. Valla, M. Lavergne, V. Beau, and L. Videau, "Design and optical characterization of a large continuous phase plate for Laser Integration Line and laser Megajoule facilities," *Appl. Opt.* **42**, 2377–2382 (2003).
- A. Adolf, A. Boscheron, A. Dulac, and E. Journot, "Final optics design for the Megajoule laser," in *Third International Conference on Solid State Lasers for Application to Inertial Confinement Fusion*, W. H. Lowdermilk, ed., Proc. SPIE **3492**, 44–50 (1999).
- H. Kogelnik, "Coupled wave theory for thick holographic gratings," *Bell Syst. Tech J.* **48**, 2909–2947 (1969).
- T. K. Gaylord and M. G. Moharam, "Analysis and applications of optical diffraction by gratings," in Proc. IEEE **73**, 894–937 (1985).
- Grating Solver Development Company, P.O. Box 353, Allen, Texas, 75013.
- Flow Interferogram Processing, software developed by SAGEM St Pierre du Perray, Avenue de la Tour Maury, 91280 St Pierre du Perray, France.
- D. Malacara, M. Servin, and Z. Malacara, *Interferogram Analysis for Optical Testing* (Marcel Dekker, New York), pp. 285–335.
- A. Liard, M. Bray, and G. Chabassier, "Laser megajoule optics: II. Wavefront analysis in the testing of large components," in

- Optical Fabrication and Testing*, R. Geyl and J. Maxwell, eds., Proc. SPIE **3739**, 461–473 (1999).
14. Société Européenne des Systèmes Optiques, Pôle d'activité d'Aix les Milles, 305 rue L. Armand, BP55000, 13792 Aix en Provence Cedex 3, France.
 15. J. Hue, J. Dijon, G. Ravel, P. Lyan, P. Garrec, T. Lanternier, M. Olivier, and A. Lagrande, "Automatic YAG damage test benches: additional possibilities," in *Laser-Induced Damage Threshold in Optical Materials: 1998*, G. J. Exarhos, A. H. Guenther, M. R. Kozlowski, K. L. Lewis, and M. J. Soileau, eds., Proc. SPIE **3578**, 290–301 (1998).
 16. J. H. Campbell, F. Rainer, M. R. Kozlowski, C. R. Wolfe, I. M. Thomas, and F. P. Milanovitch, "Damage resistant optics for a megajoule laser," in *Laser-Induced Damage Threshold in Optical Materials: 1990*, H. E. Bennett, L. L. Chase, A. H. Guenther, B. E. Newnam, M. J. Soileau, eds., Proc. SPIE **1441**, 444–456 (1990).
 17. H. Bercegol, P. Bouchut, L. Lamaignere, B. Le Garrec, and G. Raze, "The impact of laser damage on the lifetime of optical components in fusion lasers," in *Laser-Induced Damage Threshold in Optical Materials: 2003*, G. J. Exarhos, A. H. Guenther, N. Kaiser, K. L. Lewis, M. J. Soileau, and C. J. Stolz, eds., Proc. SPIE **5273**, 312–324 (2004).
 18. H. T. Nguyen, B. W. Shore, S. J. Bryan, J. A. Britten, R. D. Boyd, and M. D. Perry, "High efficiency fused-silica transmission gratings," *Opt. Lett.* **22**, 142–144 (1997).